Pergamon

Int. J. Heat Mass Transfer. Vol. 38, No. 8, pp. 1329–1345, 1995

0017–9310/95 $9.50+0.00

0017–9310(94)00271–1

Thermoacoustic waves in a semi-infinite medium

YUFENG HUANG and HAIM H. BAU†

Department of Mechanical Engineering and Applied Mechanics, University of Pennsylvania, Philadelphia, PA 19104-6315, U.S.A.

(*Received* 7 *February* 1994 *and in final form* 22 *August* 1994)

Abstract—The generation and transmission of planar, thermoacoustic (TAC) waves by the heating of a quiescent, isothermal, semi-infinite, gaseous medium's boundary is investigated theoretically. For step and gradual changes in the boundary temperature of a $Pr = 3/4$ gas, long- and short-time asymptotes are derived for the pressure, velocity and temperature fields and for the wall heat flux. Then the method of Laplace transform with numerical inversion is used to solve the linearized equations for general wall heating conditions. By comparing the Laplace transform predictions with the asymptotic results and with experimental data, the numerical scheme is verified and found to be highly accurate. Finally, the nonlinear equations are solved numerically to assess their effect on wave characteristics and to determine the conditions under which the linear approximation is adequate.

1. INTRODUCTION

When the boundary of a compressible material (i.e. gas) is subjected to a rapid temperature change, a sudden expansion of the material will occur, which in turn will generate a pressure wave. These thermally-generated waves are referred to as thermoacoustic (TAC) waves. They propagate at approximately the speed of sound within the medium and gradually damp out because of heat and viscous diffusion.

Early interest in thermoacoustic waves was motivated by the desire to understand their contribution to sound generation (see, for example, the reviews of the literature on Rijke and Sondhauss acoustic oscillations by Feldman [1, 2] and on other sources of thermoacoustic noise by Dowling [3]). More recently, the contribution of TAC waves to heat transport has attracted interest in the space science community (i.e. [4–10]). TAC waves enhance heat transfer by converting thermal energy into compression work and by inducing convective motion away from the heated surface. This mode of heat transport has been deemed to be of particular importance in the space environment, where other modes of transport, such as natural convection, may be absent.

Our purpose in pursuing the present investigation was two-fold. We not only were interested in bettering our understanding of the contribution of TAC waves to the heat transfer process in general, but also in exploring the possible role of TAC waves in two instrumentation-related applications. More specifically, we were interested in the potential use of thermal actuators for the generation of high amplitude acoustic waves. By measuring the speed of propagation of such waves, one can infer various gas properties such as average molecular mass, composition or temperature. Additionally, we wished to evaluate the contribution of TAC waves to noise problems, which adversely affect the performance of thermal conductivity sensors measuring the conductivity of flowing gases. These sensors are often used in gas chromatography, and they typically consist of a constant temperature filament embedded in a constant temperature channel. The thermal conductivity of the gas is inferred from the filament's power consumption. When the flowing, colder gas encounters the hot filament, a sudden expansion of the gas occurs which, in turn, induces TAC waves. These continuously generated waves cause time-dependent heat transfer from the filament and thus adversely impact the thermal conductivity measurement. Before addressing the somewhat more difficult problem of TAC waves in a moving gas, we study here the simpler problem of TAC waves in a quiescent medium.

There are just a few experimental studies that focus on TAC waves. At a point inside a closed cylinder, one end of which was subjected to a sudden temperature change, Parang and Salah-Eddine [10] measured the temperature as a function of time and demonstrated that TAC waves enhance thermal mixing. Brown [11] and Brown and Churchill [12, 13] measured pressure as a function of time. However, no direct measurements of heat transfer were made.

Analytical investigations of TAC waves date back to Lord Rayleigh [14], who carried out a linear analysis. This analysis was expanded upon by Trilling [15], who used the Laplace transform method to obtain a long-time asymptote for a thermally induced pressure wave in a semi-infinite medium subjected to a step change in wall temperature. More recently, Kassoy

† Author to whom correspondence should be addressed.

NOMENCLATURE

a speed of sound
A the magnitude of the change in the wall's temperature
C_p, C_v specific heats at constant pressure and at constant volume
P pressure
Pr Prandtl number
q wall heat flux
s Laplace variable
t time
T temperature
T_w wall temperature
y coordinate normal to the wall
V velocity in the y direction.

Greek symbols
α thermal diffusivity
γ ratio of specific heats
η $y/2\sqrt{t}$
μ dynamic viscosity
ν kinematic viscosity
ρ density
σ Bromwich line's location
τ time delay
χ norm determining the difference between two functions.

Superscripts
$*$ dimensional quantities
$\sim$ transformed variable.

Subscript
0 quiescent conditions.

Abbreviations
ILT inverse Laplace transform
FD finite difference
LW linear wave
NLWTI nonlinear wave with temperature-independent thermophysical properties
NLWTD nonlinear wave with temperature-dependent thermophysical properties
TAC thermoacoustic wave.

[6] and Radhwan and Kassoy [9] used boundary layer analysis to investigate one-dimensional, nonlinear TAC waves transmitted in a confined medium. The aforementioned analyses covered only limiting cases.

In order to obtain general solutions, a number of researchers [4, 5, 7, 8, 11] have studied numerically one- and two-dimensional TAC waves in a confined region. All these investigators used finite differences with the convective derivatives being approximated by a first-order upwinding scheme and with crude grid spacing relative to the length scale of the acoustic wave at short times. The results of all the aforementioned numerical simulations are in good agreement with each other. Unfortunately, as Brown [11] noted, the numerical results do not resemble his experimental observations. Among other things, we will investigate here whether this lack of agreement between experiment and theory is due to deficiencies in the mathematical model or due to numerical imprecision.

In this paper, we investigate theoretically one-dimensional, TAC waves transmitted in a semi-infinite medium. In a subsequent paper [16], we study TAC wave transmission in a confined medium. Here, we start by studying the linear problem in a semi-infinite medium using the Laplace transform method. First, we consider TAC waves generated by a step change in the wall temperature. While such step changes are physically unrealistic, it is useful to examine this idealized situation since it enables us to generate long- and short-time asymptotic approximations. The long-time asymptotes are also valid for situations in which the wall has thermal inertia and its temperature increase is gradual. Next, we invert the Laplace transform numerically and verify the numerical method by comparing its predictions with the asymptotic solutions. The numerical inversion technique allows us to compute wave propagation for general wall temperature variations. This numerical method has the advantage over finite differences/elements that it is not sensitive to grid spacing and artificial dissipation. Consequently, it allows one to obtain highly accurate results. Then, we investigate the effect of the wall's heating rate on the nature of the TAC waves. Subsequently, we compute the nonlinear TAC waves using finite differences and finite elements. Unfortunately, to maintain high precision, these schemes require very small time-steps. This limits the computations to relatively short times. The nonlinear results are compared with the linear theory's predictions to assess the effect of nonlinearities on the wave characteristics and to establish the conditions when nonlinear effects can be neglected. Finally, we compare our theoretical results with Brown's [11] experimental data.

2. THE MATHEMATICAL MODEL

Consider a rigid wall in contact with a compressible, ideal gas (Fig. 1). The gas is initially quiescent at a uniform pressure (P_0^*) and temperature (T_0^*). Properties corresponding to the quiescent state are denoted by a subscript zero. Superscript (*) denotes dimensional quantities. As a result of a change in the boundary temperature, $T_w^*(t)$, deviations from quiescent values will occur. We denote the non-dimensional velocity, density, pressure and temperature deviations by V, ρ, P and T, respectively.

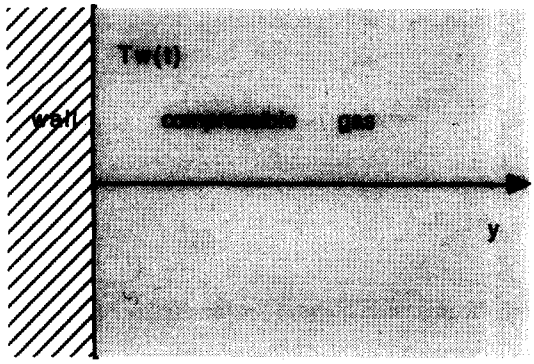

Fig. 1. Schematic description of the problem and the coordinate system.

The continuity, momentum, energy, and state equations for one-dimensional, TAC waves are, respectively,

$$\frac{\partial \rho}{\partial t}+\frac{\partial V}{\partial y}+\frac{\partial(\rho V)}{\partial y}=0 \tag{1}$$

$$(1+\rho)\frac{\mathrm{D}V}{\mathrm{D}t}=-\frac{1}{\gamma}\frac{\partial P}{\partial y}+\frac{1}{\gamma}\frac{\partial}{\partial y}\left[\frac{\mu^*(T)}{\mu_0^*}\frac{\partial V}{\partial y}\right] \tag{2}$$

$$(1+\rho)\frac{\mathrm{D}T}{\mathrm{D}t}+(\gamma-1)(P+1)\frac{\partial V}{\partial y}$$

$$=\frac{3}{4Pr}\frac{\partial}{\partial y}\left[\frac{k^*(T)}{k_0^*}\frac{\partial T}{\partial y}\right]+(\gamma-1)\frac{\mu^*(T)}{\mu_0^*}\left(\frac{\partial V}{\partial y}\right)^2 \tag{3}$$

and

$$P=\rho+T+\rho T. \tag{4}$$

The boundary and initial conditions are:

$$T(0,t)-T_w(t)=V(0,t)=T(\infty,t)=V(\infty,t)=0 \tag{5}$$

and

$$T(y,0)=\frac{\partial T}{\partial t}(y,0)=V(y,0)=\frac{\partial V}{\partial t}(y,0)=0. \tag{6}$$

In the above

$$\frac{\mathrm{D}}{\mathrm{D}t}=\frac{\partial}{\partial t}+V\frac{\partial}{\partial y}$$

Pr is the Prandtl number; and

$$\gamma=\frac{C_p^*}{C_v^*}$$

is the ratio of the specific heats, which we assumed to be temperature-independent. For example, for helium between 3 and 900 K, C_p^* is constant; and for nitrogen between 220 and 600 K, C_p^* changes by about 4% [17]. All variables were nondimensionalized. P_0^* is the pressure scale. T_0^* is the temperature scale. ρ_0^* is the density scale. $a_0^*=\sqrt{\gamma R T_0^*}$, the sound speed in the undisturbed gas, is the velocity scale.

$$\tfrac{4}{3}\gamma\frac{\mu_0^*}{\rho_0^* a_0^*}$$

is the length scale, where μ_0^* is the viscosity.

$$\tfrac{4}{3}\gamma\frac{\mu_0^*}{\rho_0^*(a_0^*)^2}$$

is the time scale. We neglected buoyancy since, even if buoyant forces were present, the time scale associated with the buoyant flow would be much larger than that of the acoustic wave [5].

3. THE LINEAR MODEL

In the first part of this paper, we assume that the TAC wave causes only small disturbances in the quiescent state. Thus, we neglect nonlinear terms in the equations. The conditions when the linear model is valid will be established later in the paper. The nondimensional, linearized equations are:

$$\frac{\partial \rho}{\partial t}+\frac{\partial V}{\partial y}=0 \tag{7}$$

$$\frac{\partial V}{\partial t}=-\frac{1}{\gamma}\frac{\partial P}{\partial y}+\frac{1}{\gamma}\frac{\partial^2 V}{\partial y^2} \tag{8}$$

$$\frac{\partial T}{\partial t}-(\gamma-1)\frac{\partial \rho}{\partial t}=\frac{1}{\frac{4}{3}Pr}\frac{\partial^2 T}{\partial y^2} \tag{9}$$

and

$$P=\rho+T. \tag{10}$$

The velocity (V) and density (ρ) can be eliminated from equations (7)–(10) to obtain two coupled equations for the pressure and temperature:

$$(\gamma-(\gamma-1)\tfrac{4}{3}Pr)\frac{\partial^2 P}{\partial t^2}-\frac{\partial^2 P}{\partial y^2}$$

$$-\frac{\partial^3 P}{\partial y^2\,\partial t}-\gamma(1-\tfrac{4}{3}Pr)\frac{\partial^2 T}{\partial t^2}=0 \tag{11}$$

and

$$\frac{\partial^4 T}{\partial y^4}+\frac{\partial^5 T}{\partial y^4\,\partial t}-\tfrac{4}{3}Pr\,\gamma\frac{\partial^3 T}{\partial y^2\,\partial t}=(\tfrac{4}{3}Pr+\gamma)\frac{\partial^4 T}{\partial y^2\,\partial t^2}$$

$$-\tfrac{4}{3}Pr\,\gamma\frac{\partial^3 T}{\partial t^3}. \tag{12}$$

Equations (11) and (12) are also coupled through the boundary conditions, which we do not write explicitly here.

The special case of $Pr=3/4$ affords a simplification in the mathematical treatment, since for $Pr=3/4$ the temperature equation (12) can be factored [15]. Many gases have Prandtl numbers around 3/4 (i.e. at 300 K, air and H_2 have the Prandtl number of 0.71; that of CO_2 is 0.77). Therefore, we shall restrict the discussion in this paper to $Pr=3/4$. For $Pr=3/4$, equation (12) can be rewritten as:

$$(L_1 L_2)T = 0 \tag{13}$$

where

$$L_1 = \frac{\partial^2}{\partial t^2} - \frac{\partial^2}{\partial y^2} - \frac{\partial^3}{\partial y^2 \partial t}$$

and

$$L_2 = \gamma \frac{\partial}{\partial t} - \frac{\partial^2}{\partial y^2}.$$

Next, T is decomposed into pressure mode, T_1, and thermal mode, T_2:

$$T = T_1 + T_2 = (1-\gamma)\frac{\partial \varphi_1}{\partial t} + \gamma \varphi_2 \tag{14}$$

where

$$L_1(\varphi_1) = 0 \quad \text{and} \quad L_2(\varphi_2) = 0. \tag{15}$$

All other variables are written as a superposition of these two modes, i.e. $P = P_1 + P_2$, $\rho = \rho_1 + \rho_2$ and $V = V_1 + V_2$, where

$$P_1 = \left(\frac{\partial^2}{\partial y^2} - \gamma \frac{\partial}{\partial t}\right)\varphi_1 \quad P_2 = 0$$

$$\rho_1 = \left(\frac{\partial^2}{\partial y^2} - \frac{\partial}{\partial t}\right)\varphi_1 \quad \rho_2 = -\gamma \varphi_2$$

$$V_1 = \frac{\partial}{\partial y}\varphi_1 \quad V_2 = \frac{\partial}{\partial y}\varphi_2. \tag{16}$$

Applying the Laplace transform to the equations (15) with the initial conditions (6), we obtain

$$s^2 \tilde{\varphi}_1 = (s+1)\frac{\partial^2 \tilde{\varphi}_1}{\partial y^2} \quad \text{and} \quad \gamma s \tilde{\varphi}_2 = \frac{\partial^2 \tilde{\varphi}_2}{\partial y^2} \tag{17}$$

where s is the Laplace variable and the transformed quantities are denoted with a tilde.

By solving these equations (17), we obtain the transformed temperature, velocity and pressure:

$$\tilde{T} = (1-\gamma)s\tilde{\varphi}_1 + \gamma \tilde{\varphi}_2 \tag{18}$$

$$\tilde{V} = \frac{\partial \tilde{\varphi}_1}{\partial y} + \frac{\partial \tilde{\varphi}_2}{\partial y} \tag{19}$$

and

$$\tilde{p} = \frac{\partial^2 \tilde{\varphi}_1}{\partial y^2} - \gamma s \tilde{\varphi}_1 \tag{20}$$

where

$$\tilde{\varphi}_1(y,s) = \frac{-\sqrt{\frac{1+s}{s}}\,\tilde{T}_w(s)}{(\gamma-1)\sqrt{s(1+s)}+\sqrt{\gamma}} \exp\left(-\frac{sy}{\sqrt{1+s}}\right) \tag{21}$$

and

$$\tilde{\varphi}_2(y,s) = \frac{\tilde{T}_w(s)}{(\gamma-1)\sqrt{s(1+s)}+\sqrt{\gamma}} \frac{1}{\sqrt{\gamma}} \exp(-y\sqrt{\gamma s}). \tag{22}$$

For example, the Laplace transform for the pressure is

$$\tilde{P}(y,s) = \frac{\left(\gamma - \frac{s}{1+s}\right)\sqrt{s(1+s)}}{(\gamma-1)\sqrt{s(1+s)}+\sqrt{\gamma}} \tilde{T}_w(s) \times \exp\left(-\frac{sy}{\sqrt{1+s}}\right) \tag{23}$$

and the inversion integral for the pressure is

$$P(y,t) = \frac{1}{2\pi i}\int_{\sigma-i\infty}^{\sigma+i\infty} \tilde{P}(y,s)\,e^{st}\,ds \tag{24}$$

where $\sigma \geqslant 0$ is the location of the Bromwich line.

4. A STEP-CHANGE IN WALL TEMPERATURE: LONG AND SHORT TIME ASYMPTOTES

We derive long- and short-time asymptotic solutions for the TAC wave in a semi-infinite medium subjected to a step change of magnitude A in the wall temperature:

$$T_w(t) = \begin{cases} 0 & \text{for } t \leqslant 0 \\ A & \text{for } t > 0 \end{cases} \quad \text{and} \quad \tilde{T}_w(s) = \frac{A}{s}. \tag{25}$$

Although an instantaneous change in the wall temperature is not realizable in practice, this case is still interesting because it allows us to generate asymptotic approximations which are also valid when the increase in the wall temperature is gradual.

4.1. *Long-time asymptote*

A long-time pressure asymptote was originally obtained by Trilling [15]. Unfortunately, Trilling's derivation suffers from a number of inaccuracies which we correct below.

For long time t, most of the contribution to the inversion integral comes from the vicinity of the singularity with the largest real part ($s = 0$). Thus,

$$P(y,t) \sim A\frac{\sqrt{\gamma}}{2\pi i}\int_{\sigma-i\infty}^{\sigma+i\infty} \times \exp\left(s(t-y)+\frac{ys^2}{2}\right)\frac{ds}{\sqrt{s}} \quad (t \to \infty). \tag{26}$$

Since there are no singularities in the RHS of the complex s plane, we select $\sigma = 0$ and substitute $s = i\lambda$ to obtain

$$P(y,t) \sim A\frac{\sqrt{\gamma}}{\pi}\int_0^\infty \exp\left(-\frac{y}{2}\lambda^2\right) \times \cos\left(\lambda(t-y)-\frac{\pi}{4}\right)\frac{d\lambda}{\sqrt{\lambda}} = \chi_1(y,t)+\chi_2(y,t) \tag{27}$$

where [18]

$$\chi_1(y,t) = \frac{\sqrt{\gamma}}{2}\left(\frac{(t-y)^2}{4y^2}\right)^{1/4} \times \exp\left(-\frac{(y-t)^2}{4y}\right) I_{-1/4}\left(\frac{(y-t)^2}{4y}\right)$$

$$\chi_2(y,t) = \operatorname{sgn}(t-y)\frac{\sqrt{\gamma}}{2}\left(\frac{(t-y)^2}{4y^2}\right)^{1/4} \times \exp\left(-\frac{(t-y)^2}{4y}\right) I_{1/4}\left(\frac{(t-y)^2}{4y}\right)$$

and $I_{\pm 1/4}$ are the modified Bessel functions of orders $(\pm\frac{1}{4})$. Note that in Trilling's expression [equation (21) in his paper], the phase $\pi/4$ is missing and there is an error in the amplitude. Equation (27) provides an approximation for the pressure field valid for all y.

When $(y-t)^2/4y \ll 1$, equation (27) can be simplified further to yield the local approximation for the wave's peak:

$$P(y,t) \sim A\frac{\sqrt{\gamma}}{2^{1/4}y^{1/4}}\frac{\Gamma(\frac{1}{4})}{2\pi}\left(1+\frac{2\pi(t-y)}{\sqrt{y}(\Gamma(\frac{1}{4}))^2} + O\left(\frac{(t-y)^{7/2}}{(4y)^{7/4}}\right)\right)\exp\left(-\frac{(y-t)^2}{4y}\right). \quad (28)$$

Similarly, we obtained expressions for the long-time temperature and velocity asymptotes (for details of the derivation, see ref. [19]):

$$T(y,t) \sim \frac{\gamma-1}{\gamma}P(y,t)+1-\operatorname{erf}\left(\frac{y\sqrt{\gamma}}{2\sqrt{t}}\right) \quad (t\to\infty) \quad (29)$$

and

$$V(y,t) \sim \frac{1}{\gamma}P(y,t)-\frac{1}{\sqrt{\gamma\pi t}}\exp\left(-\frac{\gamma y^2}{4t}\right) \quad (t\to\infty) \quad (30)$$

where $P(y,t)$ is given in equation (27) and erf is the error function.

The long-time asymptote for the heat flux was obtained by computing the transformed flux and then inverting the resulting expression to obtain

$$q(t) = -\left(\frac{\partial T}{\partial y}\right)_{y=0} \sim A\sqrt{\frac{\gamma}{\pi t}}. \quad (31)$$

Equation (31) shows that the heat flux is larger by a factor of $\sqrt{\gamma}$ than the pure conduction heat flux in an incompressible medium, $q(t) = A(\pi t)^{-1/2}$. This increase in heat transfer is due to the conversion of heat into compression work resulting from the thermal expansion of the gas.

To see where this augmentation in heat transfer comes from, it is instructive to obtain equation (31) directly from equations (7)–(10). At long time ($t \gg y$), the pressure $P \sim 0$ and the density $\rho \sim -T$ [from equation (10)]. Upon substituting ρ and $Pr = 3/4$ in equation (9), we obtain

$$\gamma\frac{\partial T}{\partial t} = \frac{\partial^2 T}{\partial y^2}.$$

The heat flux predicted by this equation is given in equation (31). Thus, the heat transfer in the compressible gas is equivalent to the heat transfer in an incompressible gas with the thermal capacity increased by a factor of γ.

4.2. *Short-time asymptote*

Next, we obtain short-time asymptotes ($t \to 0$). The procedure consists of expanding the integrand in equation (24) in a series of negative powers of the Laplace variable, s. We omit the details of our derivation and refer the interested reader to Huang [19]. The short-time approximations for the temperature field, velocity field, and wall heat flux are:

$$T(t,y) \sim A\{\zeta_1(\eta)-t(\zeta_3(\eta)-\zeta_3(\sqrt{\gamma}\eta))\}+O(t^2) \quad (32)$$

$$V(t,y) \sim A\frac{\sqrt{t}}{(\gamma-1)}(\zeta_2(\eta)-\zeta_2(\eta\sqrt{\gamma}))+O(t) \quad (33)$$

and

$$q(t) \sim \frac{A}{\sqrt{\pi t}}\left(1+\frac{\sqrt{\gamma}-1}{\sqrt{\gamma}+1}t+O(t^2)\right) \quad (34)$$

where

$$\eta = \frac{y}{2\sqrt{t}} \qquad \zeta_1(\eta) = 1-\operatorname{erf}(\eta)$$

$$\zeta_2(\eta) = \frac{2}{\sqrt{\pi}}e^{-\eta^2}-2\eta\zeta_1(\eta)$$

and

$$\zeta_3(\eta) = \frac{\sqrt{\gamma}}{\gamma-1}\{\zeta_1(\eta)-\eta\zeta_2(\eta)\}.$$

For very short times, the phenomenon is dominated by conduction; $\zeta_1(\eta)$ is the conductive temperature field and the first term in equation (34) is the conductive heat flux.

5. A GRADUAL CHANGE IN WALL TEMPERATURE: LONG AND SHORT-TIME ASYMPTOTES

Thus far, we have considered TAC waves generated by a step change in the wall temperature. In practice, as a result of the wall and heater thermal inertias and heat losses to the environment, it is not possible to generate a step change in the wall temperature. We approximate the dependence of the wall temperature on time by the exponential expressions

$$T_w(t) = A\left(1-\exp\left(-\frac{t}{\tau}\right)\right)$$

and

$$\tilde{T}_w(s) = A\left(\frac{1}{s}-\frac{\tau}{s\tau+1}\right) \tag{35}$$

where τ is the heating process' time constant. A step change in the wall temperature (Section 4) corresponds to $\tau = 0$.

5.1. *Short-time asymptote*

To compute short-time asymptotes, we utilize a technique similar to the one described in Section 4.2. See ref. [19] for details. For example, the short-time asymptote ($t/\tau \ll 1$) for the wall heat flux is

$$q(t;\tau) \sim \frac{A}{\sqrt{\pi t}}\left(\frac{t}{\tau}\right)\left(2+\frac{4}{3}\frac{\sqrt{\gamma}}{\sqrt{\gamma}+1}t+O(t^2)\right)\left(\frac{t}{\tau}\to 0\right). \tag{36}$$

Witness that $q(0) = 0$. This is in contrast with the less realistic case of a sudden jump in the wall temperature [$\tau = 0$, equation (34)] which predicts $q(0) = \infty$.

5.2. *Long-time asymptote*

The long-time behavior of the case with $\tau > 0$ is similar to that of the case with $\tau = 0$. Below, we present the long-time asymptote for the heat flux for $\tau > 0$,

$$q(t;\tau) \sim A\sqrt{\frac{\gamma}{\pi t}}R\left(\frac{t}{\tau}\right)+O\left(\frac{\tau}{t}\right) \tag{37}$$

where $R(x) = 2x\,{}_1F_1(1,\frac{3}{2},-x)$ and ${}_1F_1$ is Kummer's confluent hypergeometric function [20] which we evaluated with the aid of Mathematica [21], whose notation we are using here. Witness that $R(0) = 0$; thus for $\tau > 0$, the long-time asymptote gives qualitatively correct results for all times. For large values of t/τ, the expression for $R(x)$ can be further simplified to

$$R(x) \sim 1+\frac{1}{2x}+\frac{3}{4x^2}+\frac{15}{8x^3}+\frac{105}{16x^4}+O(x^{-5}).$$

6. NUMERICAL INVERSION

Closed form inversion is possible only in the asymptotic limits of short and long times and for relatively simple wall temperature histories. In order to be able to deal with more general cases, we resort to numerical inversion. We use the FORTRAN routine ACM-Alg. 219 [22], which utilizes a truncated Fourier series method to compute the inversion integral. This technique has the advantage that it allows one to compute the required variables at any location and at any time without having to compute the entire flow field as would be the case if one were to use finite differences or elements. It is also free of numerical dissipation errors which plague many numerical techniques and cause artificial broadening of the acoustic signal (see, for example, Brown [11]). The discretization error of the numerical inversion is given in ref. [22].

In order to compute the inversion integral at any given (y, t), one needs to select the location (σ) of the Bromwich line. Since the integrand is free of singularities in the RHS of the complex (s) plane, we set $\sigma = 0$. We did, however, verify that the computational results are independent of the location of the Bromwich line by integrating for $\sigma = 0.01$ and 0.1. As long as $\sigma < 1$, identical results were obtained. For $\sigma > 1$, an overflow error resulted. We also verified that the computed results were independent of accuracy specifications required by the numerical code.

Finally, we verified the code by comparing the numerical inversion with an analytical one. Equation (26) has an exact invert [equation (27)]. The relative difference,

$$\varepsilon(y,t) = \frac{p_{\text{numerical}}(y,t)-p_{\text{analytic}}(y,t)}{p_{\text{analytic}}(y,t)}$$

between the numerical and analytical inversions of equation (26) is depicted in Fig. 2 as a function of (y) for nondimensional times $t = 10$, 20 and 30. The relative difference ε was always smaller than 10^{-6} (or $10^{-4}\%$), which is about the same as the accuracy we specified in the code. Figure 2 demonstrates that the numerical inversion produces reliable results for the type of problems under consideration in this paper.

7. LINEAR TAC WAVES RESULTING FROM A STEP CHANGE IN WALL TEMPERATURE ($\tau = 0$)

In this section, we describe the pressure, velocity and temperature waves in a semi-infinite medium and the wall heat flux resulting from a step change ($\tau = 0$) in the wall temperature. We use numerical inversion of the Laplace transform and, when appropriate, we compare the numerical results with long- and short-time asymptotes.

Figure 3 depicts the pressure wave (P/A) as a function of y for nondimensional times 10, 100 and 1000. The solid lines and circles describe, respectively, the numerical (exact) solutions and the long-time asymptotes. For $t < 100$, the asymptotic solution overpredicts the height of the pressure peak. As time (t) increases, the numerical and the asymptotic solutions get closer. At $t \geqslant 10^3$, there is no detectable difference between the asymptotic and exact solutions. The waves are characterized by a steep front and a relatively long 'tail'. The steep front results from the sudden expansion due to an instantaneous increase in the wall's temperature. As time increases, the wave peak broadens. The broadening is proportional to the molecular diffusion length, $\sqrt{\upsilon^* t^*}$, where υ^* is the kinematic viscosity. This feature is somewhat

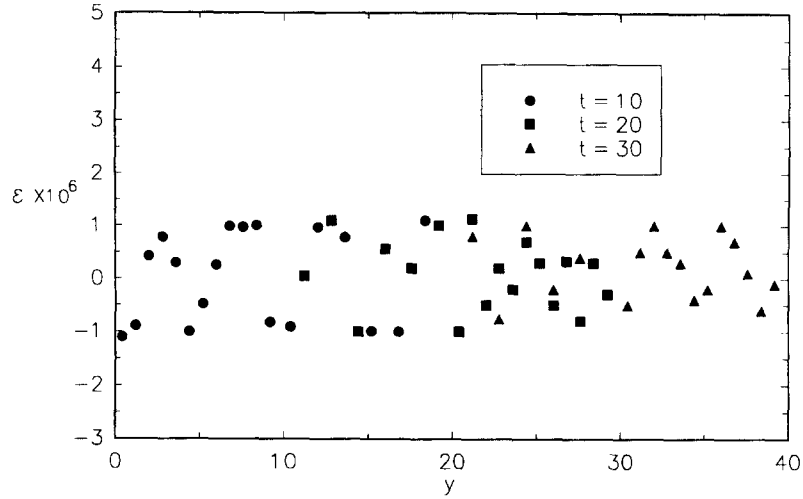

Fig. 2. Relative difference, $\varepsilon = (p_{\text{numerical}} - p_{\text{analytic}})/p_{\text{analytic}}$, between the analytical (exact) and the numerical inversions of the asymptotic expression for the TAC pressure wave in a semi-infinite medium as a function of y for times $t = 10$, 20 and 30.

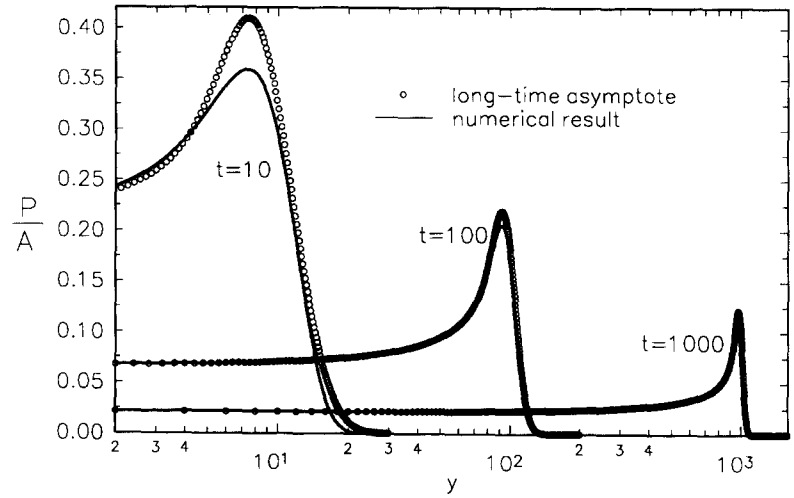

Fig. 3. The normalized pressure resulting from a step change in wall temperature is depicted as a function of y for times $t = 10$, 100 and 1000. The line and circles describe, respectively, 'exact' numerical and long-time asymptotes.

obscured in Fig. 3 because of the logarithmic scale used for the abscissa (y).

The pressure wave's amplitude as a function of time is depicted in Fig. 4 by the curve denoted $\tau = 0$. The circles and $\times$s correspond, respectively, to the numerical and long-time asymptotic results. The solid lines are least-square curve fits. The amplitude of the pressure wave decreases in proportion to the inverse fourth root of time (or distance). The numerical results are in excellent agreement with the asymptotic ones.

Figure 5 depicts the velocity, V/A, as a function of y for times $t = 0.1$, 0.5, 1, 4, 10, 30, 50 and 100. To accommodate the expansion of the gas due to the increase in the temperature, the velocity is always directed in the positive y direction and its peak is synchronized with the pressure peak. Figure 5 also depicts short-time asymptotes [equation (33)] for $t = 0.1$, 0.5 and 1 (dashed lines) and the long-time asymptotes [equation (30)] for $t = 30$, 50 and 100 (dotted lines). For $t = 0.1$, there is excellent agreement between the short-time asymptote and the exact solution. For $t = 0.5$ and $t = 1$, there are, respectively, about a 10 and a 25% difference between the short-time asymptotes and the exact solutions. The numerical solution and the long-time asymptote converge as the time increases. The magnitude of the velocity peak increases from close to zero, next to the impermeable wall ($y = 0$), to a maximum at $y \sim 5$, and then it decreases again as the wave dissipates.

Figure 6 depicts the numerically computed (solid line) and the long-time asymptote (dots) for the temperature, T/A, as a function of distance (y) for $t = 20$, 100 and 500. Observe the thermal boundary layer in the vicinity of the solid wall where the temperature drops sharply from the wall value of A to almost zero. The thickness of the boundary layer increases in

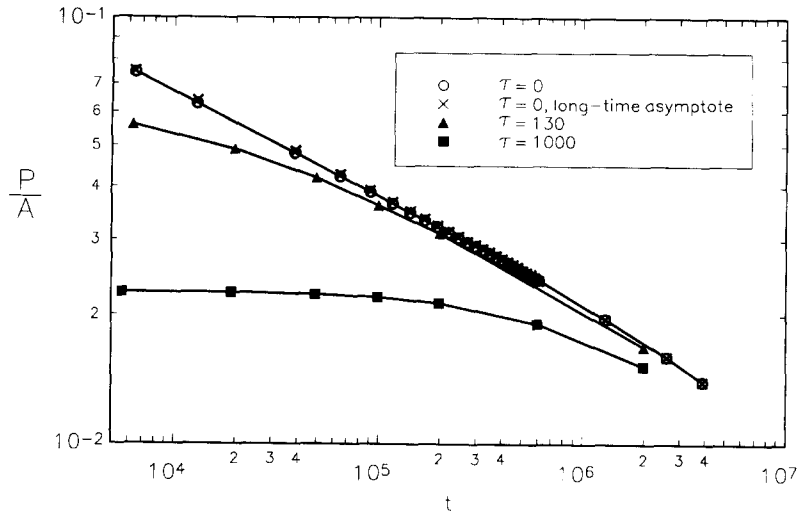

Fig. 4. The normalized pressure wave's amplitude is depicted as a function of time for a TAC wave resulting from a change in the wall's temperature with $\tau = 0$, 130 and 1000. The solid line and $\times$s correspond, respectively, to 'exact' numerical and asymptotic (only for $\tau = 0$) results. The lines are curve fits through the computed points.

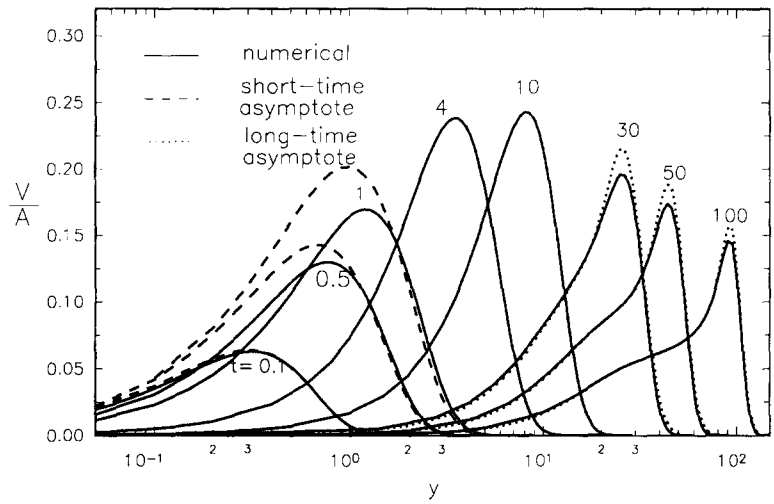

Fig. 5. The normalized velocity resulting from a step change in wall temperature is depicted as a function of y for times $t = 0.1$, 0.5, 1, 4, 10, 30, 50 and 100. The solid, dotted and dashed lines describe, respectively, numerical results, long-time asymptote, and short-time asymptotes.

proportion to $\sqrt{\alpha^* t^*}$, where α^* is the thermal diffusivity of the gas. The temperature 'hump' propagates at the speed of sound.

For example, if the medium under consideration consists of nitrogen originally at STP, the nominal speed of sound $a_0^* = 332$ m s^{-1}. The nondimensional time $t = 10^3$ and distance $y = 10^3$ correspond, respectively, to 0.2 μs and 70 μm. The wave speed, calculated from the distance covered by the pressure 'hump' in a given time, is approximately ~ 350 m s^{-1}. For $A = 1$, the first pressure peak depicted in Fig. 3 is approximately 40 kPa in magnitude.

The wall heat flux as a function of time is depicted in Fig. 7 ($\tau = 0$). The solid, dot–dashed, and dotted lines correspond, respectively, to the numerical solution, the long-time asymptote, and the short-time asymptote. The heavy, dashed line describes the heat flux due to conduction in an incompressible medium.

8. LINEAR TAC WAVES RESULTING FROM A GRADUAL CHANGE IN WALL TEMPERATURE ($\tau > 0$)

In this section, we compute the TAC waves when the wall is subjected to a gradual temperature change [equation (35), $\tau > 0$]. Figure 7 depicts the wall heat flux as a function of time (t) for $\tau = 0$, 1, 5, 13 and 130. When $\tau > 0$, $T_w(0) = 0$ and the wall heat flux $q(0) = 0$. This is in contrast to the case of the step change ($\tau = 0$), where $q(0) = \infty$. As t increases ($\tau > 0$), the wall heat flux initially increases, attains a maximum at $t \sim \tau$, and then declines. The initial

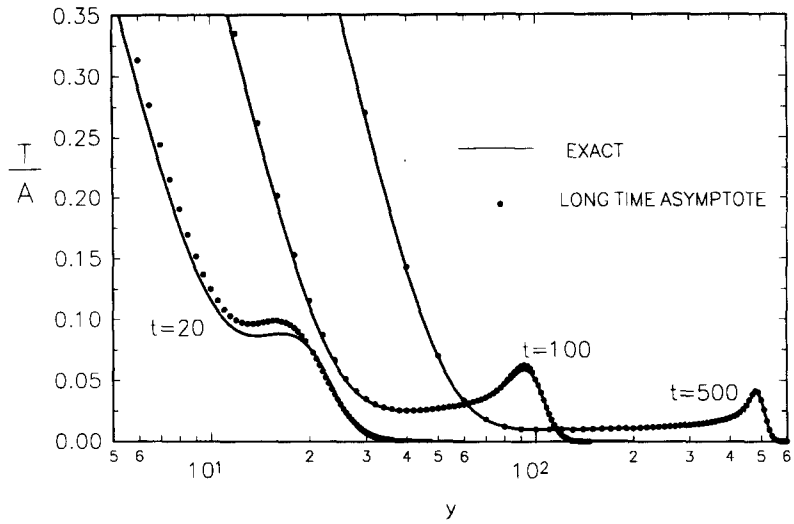

Fig. 6. The normalized temperature distribution resulting from a step change in the medium's wall temperature is depicted as a function of y for times $t = 20$, 100 and 500. The solid curves and the dots represent, respectively, numerical results and long-time asymptotes.

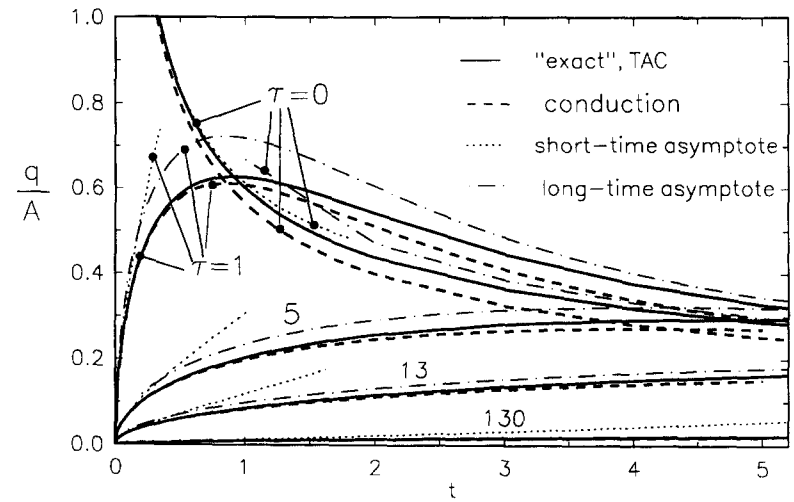

Fig. 7. The wall heat flux is depicted as a function of time for wall time constants $\tau = 0$, 1, 5, 13 and 130. The solid ('exact' numerical results), dot–dashed (long-time asymptote) and the dotted (short-time asymptote) lines depict the heat flux induced by the TAC wave. The heavy dashed line corresponds to heat flux induced by conduction alone.

increase in the heat flux is due to the increase in the wall temperature. The subsequent decline is caused by the thickening of the thermal boundary layer. A similar trend is exhibited by the conductive heat flux. For large t/τ, the heat fluxes for the cases of $\tau > 0$ and $\tau = 0$ converge to the same asymptote. The long-time asymptote predicts qualitatively correct behavior even for short times. For $\tau > 13$ and for all t, the discrepancy between the numerical solution and the long-time asymptote is smaller than 15%.

At nondimensional time $t = 6500$, Fig. 8 depicts the shape of the pressure wave as a function of the coordinate y for time constants $\tau = 0$ (step-change), 13, 130, 1300 and 13 000. When the medium is nitrogen at STP, $\tau = 1$ corresponds to 0.2 ns. As the time constant τ increases, the pressure peak broadens, its magnitude decreases, and its location moves closer to the wall. The distance between the locations of the pressure peaks generated by a sudden ($\tau = 0$) and gradual ($\tau > 0$) wall heating is approximately τ. The effect of the time constant τ on the wave amplitude is felt only for a limited time. For example, there is only a very slight difference (<2%) between the pressure wave for $\tau = 13$ ($\tau/t = 2 \times 10^{-3}$) and $\tau = 0$. This is because the pressure wave resulting from a step change ($\tau = 0$) is narrower and taller than the one when $\tau > 0$. Therefore, the former will decay faster than the latter. This situation is illustrated in Fig. 4, where we depict the amplitude of the pressure pulse as a function of y for $\tau = 0$, 130 and 1000. As t/τ increases, the curves with $\tau > 0$ approach asymptotically the one which corresponds to $\tau = 0$. In summary, at large y and

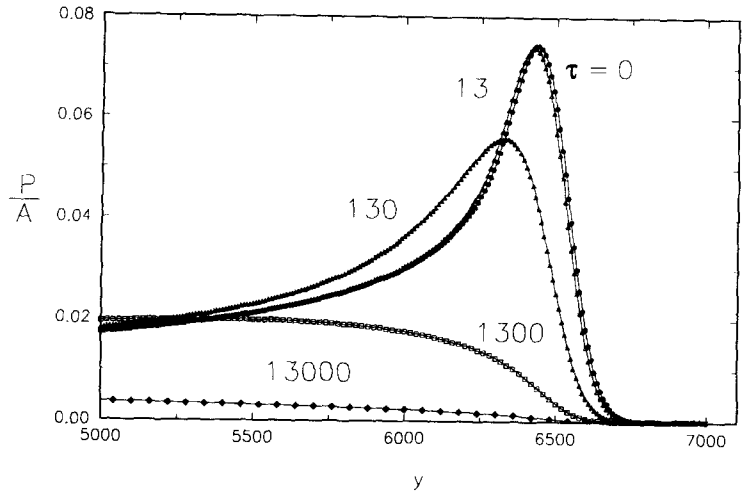

Fig. 8. The shape of the normalized pressure wave is depicted as a function of y for various wall heating rates $\tau = 0$, 13, 130, 1300 and 13 000 at $t = 6500$.

t/τ, TAC waves generated by a gradual ($\tau > 0$) wall heating induced at $t = 0$ will behave similarly to the ones generated by a sudden ($\tau = 0$) wall heating induced at $t \sim \tau$.

9. NONLINEAR EFFECTS

Thus far we have investigated linear waves. The linear analysis is strictly valid only for small amplitude waves, i.e. $Ae^{-(\tau/\tau_0)} \ll 1$, where τ_0 is estimated later in this section. Our objective is to examine the effect of nonlinearities on the wave characteristics and determine the range of validity of the linear approximation.

To this end, we solved the nonlinear equations (1)–(6) with temperature-dependent viscosity and thermal conductivity. We omitted the viscous dissipation term from equation (3) since, as we show later, in most practical situations, this term can be neglected. We approximated the nondimensional viscosity and thermal conductivity by $\mu(T) = c_1\sqrt{T}+c_2$ and $k(T) = c_3\sqrt{T}+c_4$. Unless otherwise stated, the results presented below are for nitrogen at $T_0^* = 300$ K, $c_1 = 1.489$, $c_2 = -0.489$, $c_3 = 1.66$, $c_4 = -0.66$ [17], and $Pr = 0.75$.

9.1. *The nonlinear numerical codes and their verification*

Two different numerical codes were employed to simulate the nonlinear TAC waves. The first numerical algorithm, denoted FD, consisted of a finite difference, implicit, Crank–Nicolson scheme modified with Galerkin finite element interpolation in space [23]. The convective derivatives were approximated with a truncation error $O(\Delta t^2, \Delta y^4)$, where Δy and Δt are, respectively, space and time steps. The diffusive terms were approximated using central differences to $O(\Delta y^2)$. Thus, the scheme is $O(\Delta t^2, \Delta y^2)$ accurate.

The second code was PDE2D [24, 25], which is a second-order accurate, general purpose, multi-dimensional solver for differential equations. Although both codes are unconditionally stable, to achieve the desired high precision, fairly small time steps were required. Consequently, the FD/PDE2D computations were restricted to relatively short times, i.e. $t < 10^4$. Not surprisingly, being one-dimensional, FD was significantly faster than the two-dimensional simulations with PDE2D. Therefore, most of our calculations were carried out with FD.

We verified FD and PDE2D by demonstrating the grid-size independence of the results, obtaining a good agreement between FD and PDE2D results, and computing linear TAC waves and comparing the results with the ones obtained by the inverse Laplace transform method (ILT). The relative difference between the various predictions (i.e. FD and ILT) was measured with the norm,

$$\chi_{\mathrm{ILT-FD}}(t) = \left[\frac{\int_0^\infty (P_{\mathrm{ILT}}(y,t)-P_{\mathrm{FD}}(y,t))^2\,\mathrm{d}y}{\int_0^\infty (P_{\mathrm{ILT}}(y,t))^2\,\mathrm{d}y}\right]^{1/2}. \quad (38)$$

For example, using FD with $\{\Delta y, \Delta t\} = \{0.065, 0.01\}$, we obtained $[\chi_{\mathrm{ILT-FD}}(6500) \sim 10^{-4}]$ for a pressure wave generated by a step change in the wall temperature ($\tau = 0$). Due to limitations of computer power, it was not always feasible to maintain such small time and space increments. For any other selection of time and space increments, we first solved the linear problem and verified the existence of a good agreement between FD (PDE2D) and ILT solutions. For the same choice of time and spatial steps, both FD and PDE2D yielded similar results. Further details on the verification and performance of FD and PDE2D are available in ref. [19].

9.2. *The characteristics of nonlinear waves*

In this subsection, we compare the characteristics of linear waves (LWs), nonlinear waves with tem-

perature-independent properties (NLWTIs), and nonlinear waves with temperature-dependent properties (NLWTDs). The effects of the various nonlinearities are examined in Fig. 9. At $t = 2600$, the pressure wave P/A is depicted as a function of y. Data is presented for a linear wave (dashed line, ILT, solid line, FD, and solid triangles, PDE2D); for a nonlinear wave with temperature-independent properties when $A = 1$ (thin, dotted line, FD) and $A = 2$ (thin, long dashed line, FD); and for a nonlinear wave with temperature-dependent properties when $A = 1$ (heavy dotted line, FD and solid circles, PDE2D) and $A = 2$ (heavy dashed line, FD and squares, PDE2D). Both FD and PDE2D used $\Delta y = 6.5$ and $\Delta t = 0.1$.

The various numerical schemes employed yielded similar results. For the linear wave, the FD, PDE2D, and ILT results are in a good agreement. The height of the FD and PDE2D peaks is slightly ($\sim 2\%$) lower than that of the ILT peak. $\chi_{\text{ILT-FD}} = 5 \times 10^{-3}$ and $\chi_{\text{FD-PDE2D}} \sim 3 \times 10^{-3}$. In the case of the NLWTD, we have $\chi_{\text{FD-PDE2D}} \sim 4 \times 10^{-3}$ and $\chi_{\text{FD-PDE2D}} \sim 7 \times 10^{-3}$ when $A = 1$ and 2, respectively. PDE2D appears to suffer from a slightly larger numerical dissipation than FD. Nevertheless, considering the fact that PDE2D is a general purpose, multi-dimensional program, its performance is quite impressive.

Next, we examine the effects of the various nonlinearities on the characteristics of the waves. The NLWTI propagate slightly faster and are shorter than their linear counterparts. This can be attributed to the convection increasing the temperature penetration depth into the medium and reducing the magnitude of the temperature peak. The larger A is, the faster the NLWTI moves. Doubling A increases the wave peak by only $\sim 80\%$.

The NLWTDs are taller and move faster than the NLWTIs. The NLWTD's larger amplitude is because the gas thermal diffusivity and conductivity increase with temperature. The increase in the magnitude of the diffusivity leads to a faster penetration of the temperature front into the gas which, in turn, leads to a higher peak ($\sim 25\%$) and a faster wave speed ($\sim 1.6\%$) than was the case for the NLWTI. The effect of the temperature-dependent properties is insufficient, however, to counteract the effect of the convective terms. Thus, the peaks of the NLWTDs are still shorter than those of the corresponding linear waves. Doubling A increased the peak height of the NLWTD by about 85%.

Figure 10 depicts the ILT (solid line) and FD (broken line) waves generated by a step change in the wall temperature ($\tau = 0$) as functions of y for various times. The heavy dashed line, dotted line, and light dashed line represent LW, NLWTD with $A = 1$, and NLWTD with $A = 2$, respectively. The FD grid spacing was increased gradually from $\{\Delta y, \Delta t\} = \{0.4, 0.01\}$ at $t = 260$ to $\{\Delta y, \Delta t\} = \{6.5, 0.1\}$ at $t = 5200$. The adequacy of the grid spacing is demonstrated by the good agreement between the ILT and FD results for the linear waves.

Figure 10 illustrates that the NLWTDs have a similar shape to that of the linear ones: sharp front followed by a gradual decline. The NLWTDs are shorter than their linear counterparts. The doubling of A results in less than doubling of the peak's height.

The NLWTDs propagate at a slightly higher speed than the linear waves. Figure 11 depicts the wave speed, a, as a function of time for a linear wave and NLWTDs with $A = 1$ and 2. The wave speed was determined by dividing the distance between the fronts

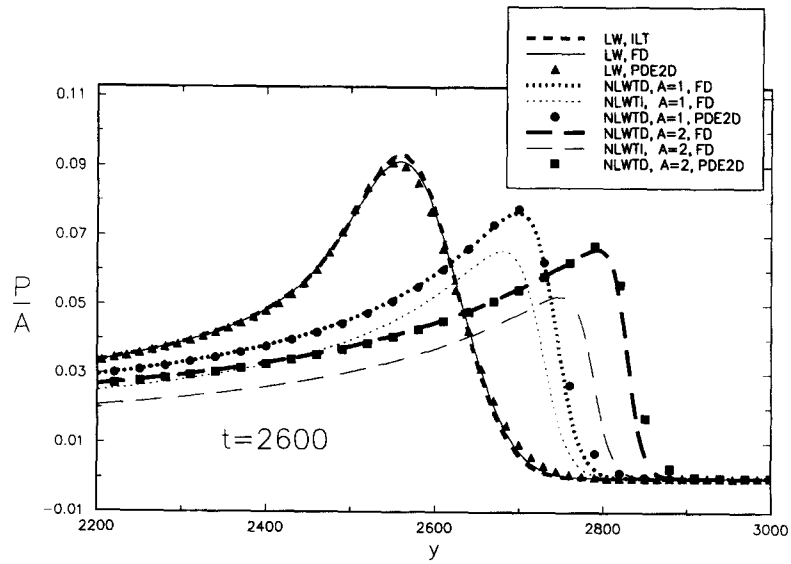

Fig. 9. At $t = 2600$, the pressure wave P/A is depicted as a function of y. Data is presented for a linear wave, LW (dashed line, ILT, solid line, FD, and solid triangles, PDE2D); for a nonlinear wave with temperature-independent properties, NLWTI, when $A = 1$ (thin, dotted line, FD) and $A = 2$ (thin, long dashed line, FD); for a nonlinear wave with temperature-dependent properties, NLWTD, when $A = 1$ (heavy dotted line, FD and solid circles, PDE2D), and $A = 2$ (heavy dashed line, FD and squares, PDE2D).

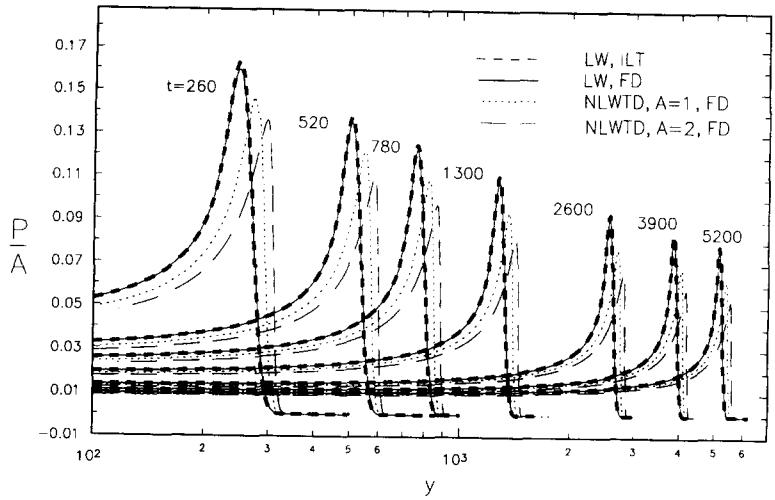

Fig. 10. As functions of y and at times $t = 260$, 520, 780, 1300, 2600, 3900 and 5200, P/A generated by a step change in the wall temperature ($\tau = 0$) is depicted as a function of time. ILT and FD results are shown with solid and broken lines, respectively. The heavy dashed line, dotted line, and light dashed line represent LW, NLWTD with $A = 1$, and NLWTD with $A = 2$, respectively.

of two peaks by the difference of the times at which the two peaks were computed. The location of the front was defined as the y coordinate of a point at 1/3 of the peak's height. At short times, the wave speeds are larger than that of the sonic speed in the undisturbed medium ($a = 1$). As A increases, so does the NLWTD's speed. As time increases, the speeds of both the NLWTD's and the LW's approach asymptotically the speed of sound in the undisturbed medium.

In Fig. 12, we compare the rate of decay of the LWs and NLWTDs. The figure depicts the magnitude of the pressure peak as a function of y for an LW (solid circles, ILT and open circles, FD) and NLWTDs with $A = 0.2$ (x), $A = 1$ (solid triangle), and $A = 2$ (open triangle). The linear pressure peak's magnitude is proportional to $y^{-\beta}$, where $\beta = \frac{1}{4}$. The nonlinear waves decay faster than their linear counterparts. When $A = 0.2$, we observe a gradual transition from $\beta \sim 0.28$ ($y < 4 \times 10^3$) to $\beta \sim 0.25$ ($y > 6 \times 10^3$). When $A = 1$ and $A = 2$, $\beta \sim 0.3$ and 0.31, respectively.

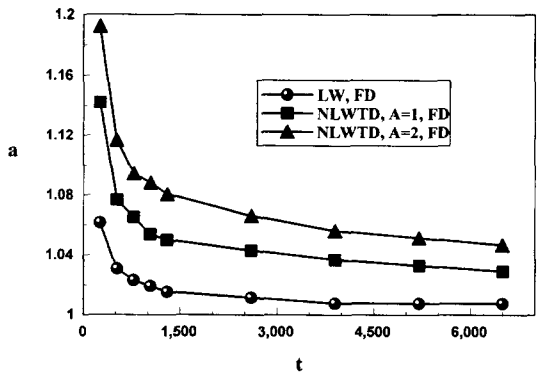

Fig. 11. The wave speed, a, is depicted as a function of time for a linear wave and NLWTDs with $A = 1$ and 2.

We speculate that for sufficiently large y, $y > y_A$ say, the nonlinear waves will behave like linear ones. The magnitude of y_A is likely to increase as A increases. Such behavior was observed for $A = 0.2$, but not for $A = 1$ and $A = 2$. This is perhaps because, in the latter cases, due to computer time limitation, we were not able to carry out the calculations for sufficiently large y values.

At $t = 100$, Fig. 13 depicts, as a function of y, the temperature distribution next to the heated wall subjected to a sudden change ($\tau = 0$) in wall temperature ($A = 1$) at $t = 0$. The heavy dashed and dotted lines describe, respectively, LW and nonlinear NLWTD waves. The heavy dotted and dashed lines correspond to conduction solutions in an incompressible medium with temperature-independent and temperature-dependent thermophysical properties. The linear wave's thermal boundary layer is thinner than the linear conduction's one because the conduction solution neglects gas expansion and the conversion of heat into work. Because of the increase in the magnitude of thermophysical properties with temperature, the thickness of the boundary layers associated with NLWTDs and nonlinear conduction are thicker than those associated with their linear counterparts. Finally, the boundary layer of the NLWTD is thicker than that of nonlinear conduction due to the effect of convection (which is not accounted for by the LW).

The wall heat flux resulting from a step change in wall temperature ($\tau = 0$) and $A = 1$ is depicted as a function of time in Fig. 14. Results are given for linear conduction (dashed–dot line) in an incompressible medium; nonlinear conduction (dotted line) in an incompressible medium; LW (solid line, ILT, and heavy dashed line, FD); and NLWTD (long dashed line). Due to the sudden increase in the wall temperature, in all cases, the heat flux at $t = 0$ is infinite. This singularity causes numerical oscillations when one is

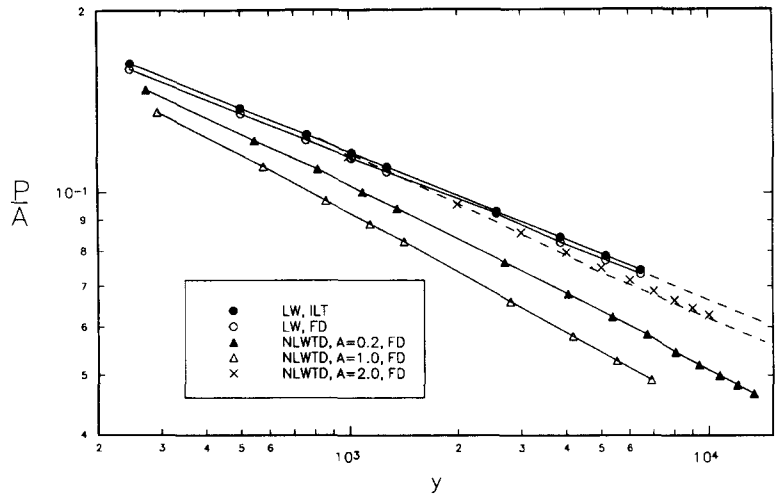

Fig. 12. The magnitude of the pressure peak is depicted as a function of y for an LW and NLWTDs with $A = 0.2$ ($\times$), $A = 1$ (solid triangle), and $A = 2$ (open triangle).

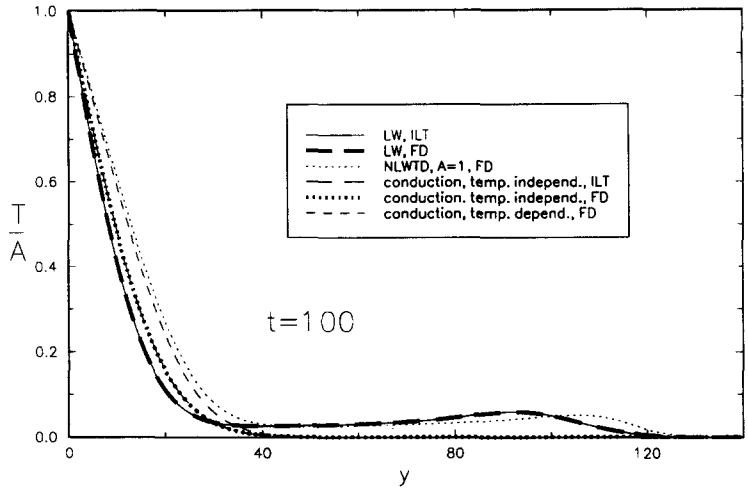

Fig. 13. At $t = 100$, the temperature distribution next to the heated wall is depicted as a function of y. The wall was subjected to a sudden change ($\tau = 0$) in temperature ($A = 1$) at $t = 0$. The heavy dashed and dotted lines describe, respectively, LW and NWLTD. The heavy dotted and dashed lines correspond to conduction solutions in an incompressible medium with temperature-independent and temperature-dependent thermophysical properties.

computing short-time heat fluxes with FD and PDE2D. The duration of these oscillations can be reduced, but not eliminated, by reducing Δt. We computed the heat flux with Δt ranging from 0.001 to 0.1 and obtained the same results for $t > 1$. A more elegant means of eliminating the singularity problem at $t = 0$ would be to endow the wall with a small time-constant ($\tau > 0$).

The heat flux associated with the LW is higher (by a factor of $\sqrt{\gamma}$) than the constant-property conduction in an incompressible medium, but slightly lower than the conductive flux when the temperature dependence of thermophysical properties is accounted for. This is, of course, because the gas' conductivity increases with temperature. At short times, such as $t < 20$ (see figure insert), due to the contribution of convection the heat flux associated with NLWTDs was higher than that of conduction with temperature-dependent properties as well as the LW. As time goes by, however, the thickness of the NLWTD's thermal boundary layer increases faster than in the absence of TAC waves, which, in turn, leads to a reduction in the heat flux below that of pure conduction.

9.3. *The range of validity of the linear approximation*

The importance of nonlinear effects depends on the magnitude of A. For example, for $A < 0.2$ and $\tau = 0$, $\chi_{\text{LW-NLWTD}}(t) < 0.05$ for $0 < t < 10^3$. In other words, when $A < 0.2$ and $\tau = 0$, the linear approximation will render results with a 5% error or smaller.

As τ increases, the amplitude of the TAC wave decreases. Thus, waves with large τ should behave like linear waves. The effect of τ is examined in Fig. 15. At $t = 200$, Fig. 15 depicts the LWs (heavy lines) and

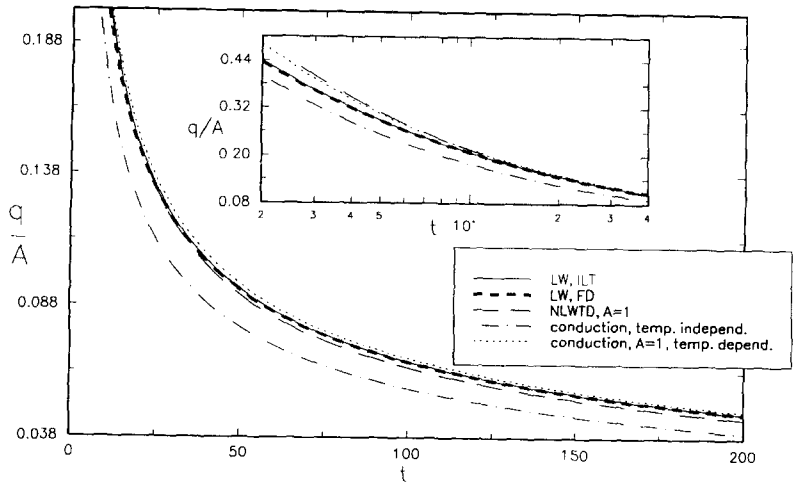

Fig. 14. The wall heat flux resulting from a step change in wall temperature ($\tau = 0$) when $A = 1$ is depicted as a function of time. Results are given for linear (dashed–dot line) and nonlinear conduction (dotted line) and for LW (solid line, ILT, and heavy dashed line, FD) and NLWTD (long dashed line).

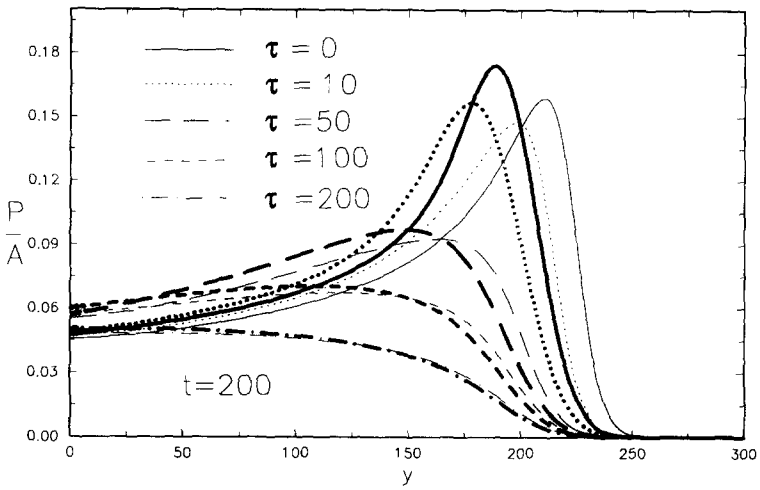

Fig. 15. At $t = 200$, P/A is depicted as a function of y for $\tau = 0$ (solid line), 10 (dots), 50 (long dashed line), 100 (short dashed line) and 200 (dashed–dot line) and $A = 1$. LWs and NLWTDs are shown, respectively, as heavy and light lines.

NLWTDs (light lines) as functions of y for $\tau = 0$ (solid line), 10 (dots), 50 (long dashed line), 100 (short dashed line), and 200 (dashed–dot line) and $A = 1$. As τ increases, the difference between the LWs and the NLWTDs decreases. The differences between the LWs and the NLWTDs are shown in Fig. 16, which depicts $\chi_{\text{LW-NLWTD}}(t = 200; \tau)$ as a function of the time-constant, τ. The curve was approximated (solid line) by a correlation of the form $\chi(t; \tau) \sim c_5 A e^{-(\tau/\tau_0)}$, where $c_5 = 0.364$ and $\tau_0 = 50$. For example, for $A = 1$ and $\tau > 100$, the linear approximation will cause an error smaller than 5%.

The expression given above is valid only for $A = 1$, and it is risky to generalize this result for all A values. Nevertheless, as the time constant increases, the error

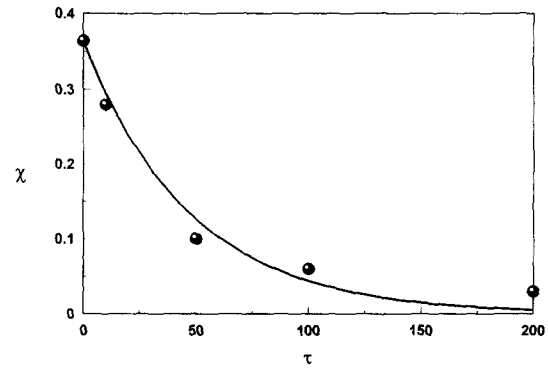

Fig. 16. $\chi_{\text{LW-NLWTD}}(t = 200; \tau)$ is depicted as a function of the time-constant, τ; $A = 1$.

incurred in using the linear approximation decreases. In many practical situations, τ is quite large. For example, in Brown's [11] experiments, $\tau \sim 10^5$. Thus, in many cases of practical importance, the linear approximation should be adequate.

The importance of nonlinear effects also diminishes as y increases. Asymptotic analysis suggests that the nonlinear, normalized contributions,

$$\left(V\frac{\partial V}{\partial y}\right)\Big/\left(\frac{\partial p}{\partial y}\right)$$

and

$$\left(V\frac{\partial T}{\partial y}\right)\Big/\left(\frac{\partial \rho}{\partial t}\right)$$

are approximately $Ay^{-1/4}$. Thus, for the convective terms to be smaller than 2% of the other terms in the equation, we need $y > (50A)^4$. For example, when $A = 0.2$, we would expect to observe linear behavior for $y > 10^4$, which is consistent with the observations made in Fig. 12.

The fact that the wave behaves linearly for large y values suggests the possibility of employing the FD scheme to obtain solutions for relatively small values of y and subsequently employing ILT for larger y with the FD results providing initial conditions for the ILT scheme.

Finally, we estimated the importance of the viscous dissipation term. For $y \sim 6000$, we find

$$\frac{\left(\frac{\partial V}{\partial y}\right)^2}{\left|\frac{\partial V}{\partial y}\right|} < 5\times 10^{-4}A.$$

Thus, in most cases of practical interest, the viscous dissipation can safely be neglected.

9.4. *Comparison with previous nonlinear solutions*

We compared our results with those of refs. [4, 5, 7, 8], all of whom employed finite differences with convective terms approximated by a first-order upwinding scheme and assumed temperature-independent thermophysical properties and no viscous dissipation. For illustration purposes, we show in Fig. 17 Ozoe *et al.*'s (ref. [8], Fig. 2) computed first peak (dotted line) of the pressure wave as a function of time at distance 0.0765 m from a heated wall ($A = 1$). Ozoe *et al.*'s calculations were performed for helium ($\gamma = 1.66$, $Pr = 0.71$) with $\Delta t \sim 5.9\times 10^4$ and $\Delta y \sim 9.5\times 10^4$ (in our nondimensional units). Due to computer power limitations, we were not able to carry out the nonlinear computations (with desired precision) for such large y values. Instead, we present in Fig. 17 our results for the linear wave (solid line) with $\gamma = 1.66$ and a slightly different Prandtl number, 0.75 instead of 0.71. In order to facilitate comparison, we shifted the time axis of Ozoe *et al.*'s data so that the location of their pressure peak coincides with ours. This shift was necessary, since their wave traveled at approximately twice the speed of sound, while our wave traveled at approximately the speed of sound in helium. Ozoe *et al.*'s pressure peak travels much faster, is much broader, has almost symmetric shape with respect to the point where the peak attains its maximum, has a smaller amplitude than our peak, and does not have the sharp front characteristic of TAC waves.

We believe that the difference between Ozoe *et al.*'s nonlinear wave and our linear one cannot be explained by nonlinearities and is a result of numerical dissipation and dispersion, and a lack of sufficient grid resolution. In the next section, we will further support this view by demonstrating that our results are in good agreement with experimental observations.

10. COMPARISON WITH EXPERIMENTS

We compare our theoretical results with Brown's [11] experimental data. Brown induced TAC waves in a 0.6 m long, closed, nitrogen-filled, plastic tube mounted vertically on a thin metal foil supported from below by a section of fibrous, ceramic insulation. The foil was heated rapidly by a RC circuit and then allowed to cool by heat losses to the environment. The foil's temperature as a function of time was measured with the aid of a thermocouple. We closely approximated Brown's foil temperature data as given in his thesis [11] using the correlation:

$$T_w(t) = \begin{cases} 1.691[1-e^{-(t^*/\tau_1^*)}] & t^* \leqslant 2.8\times 10^{-3}\ \text{s} \\ 0.209 - 2.455e^{-(t^*/\tau_2^*)} + 2.242\,e^{-(t^*/\tau_3^*)} & t^* > 2.8\times 10^{-3}\ \text{s} \end{cases} \tag{39}$$

where $\tau_1^* = 0.15$ ms ($\tau_1 \sim 10^5$), $\tau_2^* = 1.35$ ms, and $\tau_3^* = 12.6$ ms. $T_w(t)$, as given by equation (39), is depicted in Fig. 18. As a result of the heating, a TAC wave was generated and reverberated inside the tube. The induced pressure wave was measured with a microphone located at a distance of 0.305 m from the foil.

Since the theory presented here is applicable only for a semi-infinite medium while Brown's experiment was conducted in a bounded medium, we are able to predict only the first peak in his pressure measurements. The computations were carried out for the wall temperature given in equation (39). Due to computer power limitations, we were not able to compute nonlinear results for the time length required for comparison with experiments. Fortunately, given the large τ_1 value, the wave should behave linearly (Section 9.3). The ILT-predicted pressure (solid line) and the measured pressure (circles) at the microphone's location are depicted as functions of time (ms) in Fig. 18. The computed and measured pressure waves have

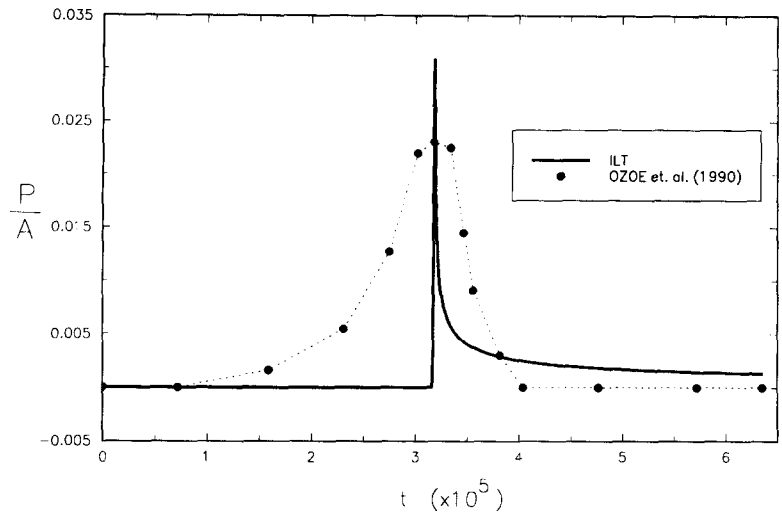

Fig. 17. Our ILT (solid line) and Ozoe *et al.*'s [8] numerical (dotted line) pressure waves are depicted as functions of time; $A = 1$.

a similar shape: a sharp front and a long 'tail'. The computed ascending part of the wave is in excellent agreement with the measurements. In the wave's trail, the computed pressure drops somewhat slower than the measured one. We speculate that the faster decay of the measured one is due to leaks in the experimental apparatus. Further credence to this speculation is given in Huang and Bau [16], where we derived a theory for confined TAC waves and were able to carry out a more complete comparison with the experiments than we can do here.

11. CONCLUSION

Using asymptotic methods and a numerically inverted Laplace transform, we have studied theoretically one-dimensional, linear TAC wave transmission in a semi-infinite, gaseous ($Pr = 3/4$) medium. Long- and short-time asymptotes were derived for the pressure, temperature, velocity waves and wall heat flux for walls subjected to sudden and gradual changes in their temperature.

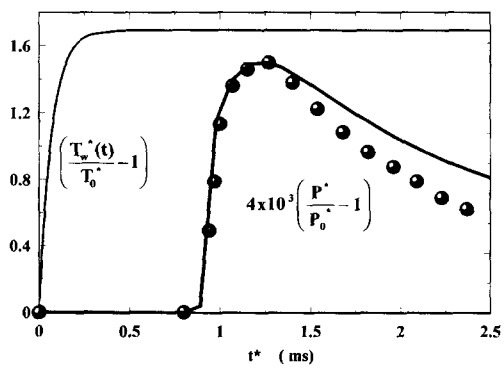

Fig. 18. A comparison between our ILT solution (solid line) and Brown's [11] experimental data (circles). The pressure wave, detected by a microphone, is depicted as a function of time (s). The figure also shows the wall temperature as a function of time.

The Laplace transform method used has the advantage of being free from numerical artifacts such as artificial dissipation and insufficient grid resolution. Comparison with asymptotic solutions indicates that the method is highly accurate. The theoretical results are also in excellent agreement with experimental data. The results presented here can, therefore, be used for benchmarking other numerical codes. The availability of such a benchmark is particularly important since the TAC wave problem is difficult to simulate accurately.

The predictions of the linear theory were compared with nonlinear solutions. The nonlinear solutions, although highly accurate, required a great amount of computer time to produce and therefore were restricted only to relatively short times. The nonlinear simulations demonstrated that the nonlinear waves damp and propagate a bit faster than their linear counterparts. The conditions when the linear approximation is valid were assessed, and it was demonstrated that in many practical situations the linear approximation is adequate. Clearly, there is a need to develop special codes which can efficiently simulate nonlinear thermoacoustic waves. An interesting alternative is the use of a hybrid scheme—finite difference solutions for short times and inverse Laplace transform for long times with the finite difference solution providing initial conditions for the inverse Laplace transform.

Acknowledgements—This work was supported in part by a grant from the Hewlett–Packard, Little Falls Division. We are grateful to HP's Dr Leonid Blumberg for his support. Dr G. Sewell from the University of Texas, El Paso, provided us with access to PDE2D and assisted us in the computations. A preliminary, abbreviated version of this paper was presented at the 1993 ASME Winter Annual Meeting [26].

REFERENCES

1. K. T. Feldman, Review of the literature on Rijke thermoacoustic phenomena, *J. Sound Vib.* **7,** 83–89 (1968).
2. K. T. Feldman, Review of the literature on Sondhauss thermoacoustic phenomena, *J. Sound Vib.* **7,** 71–82 (1968).
3. A. P. Dowling, Thermoacoustic sources and instabilities. In *Modern Methods in Analytical Acoustics* (Edited by D. G. Crighton, A. P. Dowling, J. E. Ffowcs Williams, M. Heckl and F. G. Leppington). Springer, Berlin (1992).
4. B. K. Larkin, Heat flow to a confined fluid in zero gravity, *Prog. Astrophys. Aeronaut.* **20,** 819–832 (1967).
5. L. W. Spradley and S. W. Churchill, Pressure and buoyancy driven thermal convection in a rectangular enclosure, *J. Fluid Mech.* **70,** 705–720.
6. D. R. Kassoy, The response of a confined gas to a thermal disturbance, *SIAM J. Appl. Math.* **36,** 624–634 (1979).
7. H. Ozoe, N. Sato and S. W. Churchill, The effect of various parameters on thermoacoustic convection, *Chem. Engng Commun.* **5,** 203–221 (1980).
8. H. Ozoe, N. Sato and S. W. Churchill, Numerical analyses of two and three dimensional thermoacoustic convection generated by a transient step in the temperature of one wall, *Numer. Heat Transfer A* **18,** 1–15 (1990).
9. A. M. Radhwan and D. R. Kassoy, The response of a confined gas to a thermal disturbance: rapid boundary heating, *J. Engng Math.* **18,** 133–156 (1984).
10. M. Parang and A. Salah-Eddine, Thermoacoustic convection heat-transfer phenomena, *AIAA J.* **22,** 1020–1022 (1984).
11. M. A. Brown, Thermally induced pressure wave in a gas: experimental observation and theoretical prediction of thermoacoustic convection, Ph.D. thesis, University of Pennsylvania, PA (1992).
12. M. A. Brown and S. W. Churchill, Transient behavior of an impulsively heated fluid, *Chem. Engng* **16,** 82–88 (1993).
13. M. A. Brown and S. W. Churchill, Experimental measurements of pressure waves generated in a confined gas by impulsive heating of a surface, submitted.
14. Lord Rayleigh, On the conduction of heat in a spherical mass of air confined by walls at a constant temperature, *Phil. Mag.* **47,** 314–325 (1899).
15. L. Trilling, On thermally induced sound fields, *J. Acoust. Soc. Am.* **27,** 425–431 (1955).
16. Y. Huang, and H. H. Bau, Thermoacoustic waves in a confined medium, in preparation.
17. F. Kreith and M. S. Bohn, *Principles of Heat Transfer.* Harper & Row, London (1986).
18. G. N. Watson, *A Treatise on the Theory of Bessel Functions*, p. 394. Cambridge University Press, Cambridge (1962).
19. Y. Huang, Sources of (non-electronic) noise in thermal conductivity detectors, Ph.D. dissertation, University of Pennsylvania, PA. (1995).
20. M. Abramowitz and I. Stegun (Eds), *Handbook of Mathematical Functions*, p. 504. National Bureau of Standards, Gaithersburg, MD (1964).
21. S. Wolfram, *Mathematica*, p. 578. Addison–Wesley, London (1991).
22. R. Piessens and R. Huysmans, Automatic numerical inversion of the Laplace transform, *ACM Trans. Math. Software* **10,** 348–353 (1984).
23. C. A. J. Fletcher, *Computational Techniques for Fluid Mechanics*, Vol. 1, pp. 278–279. Springer, Berlin (1991).
24. G. Sewell, *Analysis of a Finite Element Method.* Springer, Berlin (1985).
25. G. Sewell, PDE2D: easy-to-use software for general two-dimensional partial differential equations, *Adv. Engng Software* **17,** 105–112 (1993).
26. Y. Huang and H. H. Bau, Thermoacoustic convection. In *Heat Transfer in Microgravity* (Edited by C. T. Avedisian and V. A. Arpaci), pp. 13–22. HTD-269. ASME, New York (1993).